Submitted to Physics in Medicine
and Biology

LBL-8539 c.2
Preprint

3-D OBJECT RECONSTRUCTION IN EMISSION AND TRANSMISSION TOMOGRAPHY WITH LIMITED ANGULAR INPUT

RECEIVED
LAWRENCE
BERKELEY LABORATORY

MAR 13 1979

LIBRARY AND
DOCUMENTS SECTION

K. C. Tam, V. Perez-Mendez and B. Macdonald

December 1978

Prepared for the U. S. Department of Energy
under Contract W-7405-ENG-48

TWO-WEEK LOAN COPY

This is a Library Circulating Copy which may be borrowed for two weeks. For a personal retention copy, call Tech. Info. Division, Ext. 6782

LAWRENCE BERKELEY LABORATORY
UNIVERSITY OF CALIFORNIA
BERKELEY

LBL-8539 c.2

DISCLAIMER

This document was prepared as an account of work sponsored by the United States Government. While this document is believed to contain correct information, neither the United States Government nor any agency thereof, nor the Regents of the University of California, nor any of their employees, makes any warranty, express or implied, or assumes any legal responsibility for the accuracy, completeness, or usefulness of any information, apparatus, product, or process disclosed, or represents that its use would not infringe privately owned rights. Reference herein to any specific commercial product, process, or service by its trade name, trademark, manufacturer, or otherwise, does not necessarily constitute or imply its endorsement, recommendation, or favoring by the United States Government or any agency thereof, or the Regents of the University of California. The views and opinions of authors expressed herein do not necessarily state or reflect those of the United States Government or any agency thereof or the Regents of the University of California.

3-D OBJECT RECONSTRUCTION IN EMISSION AND TRANSMISSION TOMOGRAPHY WITH LIMITED ANGULAR INPUT

K. C. Tam, V. Perez-Mendez and B. Macdonald

Lawrence Berkeley Laboratory, Berkeley and Radiology Department,
U.C. San Francisco

ABSTRACT

The effects of the angular range of data taking in reconstructions in planar positron cameras using the deconvolution method and the matrix method, respectively, are investigated. It is found that in the absence of any a priori information there are undetermined components in the reconstruction if the point response function of the positron camera does not satisfy certain criteria. However, most of the undetermined components are recovered in the case in which the transverse spacing of the object is discrete, and all of them are recovered if the fact that the object extent is finite is utilized. It is concluded that the two reconstruction methods are mathematically equivalent. The results obtained can be applied to other transmission and emission imaging devices.

3-D Object Reconstruction in Emission and Transmission Tomography with Limited Angular Input

K.C. Tam, V. Perez-Mendez and B. Macdonald

I. Introduction

In radiology and nuclear medicine imaging, information on an object is usually inferred from the radiation transmitted through or emitted from the object. Such methods of imaging medical disorders, known as transmission and emission imaging, respectively, usually involve collecting the radiation events while viewing the object in a continuous range of angle or series of discrete angles, and then reconstructing the object distribution from the data. Object distribution can be two-dimensional, such as in ring positron cameras [1] and x-ray scanning (parallel beam or fan beam geometry) [2,3], as shown in Figure 1, or three-dimensional as in planar positron cameras [4] and pinhole imaging [5], as shown in Figure 2. Similar techniques have also been employed in other non-medical imaging situations, such as electron microscopy, radioastronomy, etc. In this paper we investigate the relationship between the angular range of the input data and the possibility of reconstructing the object distribution completely. Practical ways of implementing such ideas numerically are also given. In the following discussion we shall study the typical problem of imaging in planar positron cameras. The results obtained can be applied to other problems after simple modifications, as shown in Section IV.

II. Basic Equation and Methods of Solving

We shall take the line joining the centers of the two detectors of the planar positron camera as the z-axis. Due to the symmetry of the x and y axes, we shall write out only the x-axis explicitly and suppress the y-axis in most of the mathematical treatment and figures in order to facilitate presentation.

As shown in previous papers [6,7], the data in a positron camera consist of straight lines defined by the annihilation gamma pairs, with the position of the radioactive nuclide which has just undergone the β^+ decay lying somewhere along the straight line. If the number of these straight lines becomes large, they will form a scalar field $\phi(\underline{r})$ in space. If the response at $\underline{r}$ due to a point source at $\underline{r}'$ is $\phi_o(\underline{r},\underline{r}')$, then we can write

$$\phi(\underline{r}) = \int \rho(\underline{r}')\phi_o(\underline{r},\underline{r}')d^3r' \qquad (1)$$

where $\rho(\underline{r}')$ is the radioisotope distribution giving rise to the annihilation gamma pairs. Equation (1) is the basic integral equation relating the data to the object distribution.

Equation (1), as it stands, is not easy to deal with in general. However, if the kernel is space invariant, ie.

$$\phi(\underline{r}) = \int \rho(\underline{r}')\phi_o(\underline{r}-\underline{r}')d^3r' \qquad (2)$$

solving for $\rho(\underline{r})$ becomes much easier, as various methods of solving integral equations with kernels of such form have been developed [8]. Various ways of constructing the function ϕ_o and making it space invariant have been given in previous papers [6,7].

To solve Equation (2), one approach is to Fourier transform the equation to frequency space. As shown in [8], the transformed equation is diagonal, so the integral equation reduces to an algebraic equation,

$$\Phi(\underline{k}) = \Phi_o(\underline{k})R(\underline{k}) \qquad (3a)$$

where

$$\Phi_o(\underline{k}) = \int \phi_o(\underline{r})\exp(2\pi i\underline{k}\cdot\underline{r})d^3r$$

$$\Phi(\underline{k}) = \int \phi(\underline{r})\exp(2\pi i\underline{k}\cdot\underline{r})d^3r$$

$$R(\underline{k}) = \int \rho(\underline{r})\exp(2\pi i\underline{k}\cdot\underline{r})d^3r$$

The solution is given by

$$\rho(\underline{r}) = \int R(\underline{k})\exp(2\pi i\underline{k}\cdot\underline{r})d^3k \qquad (3b)$$

where

$$R(\underline{k}) = \begin{cases} \dfrac{\Phi_o(\underline{k})}{\Phi_o(\underline{k})} & \text{if } \Phi_o(\underline{k}) \neq 0 \\ \text{undetermined} & \text{if } \Phi_o(\underline{k}) = 0 \end{cases} \qquad (3c)$$

(since here Equation (3a) becomes 0 = 0)

If we Fourier transform Equation (2) only in the x dimension, we get the equation

$$\varphi(k_x,z) = \int_{-\infty}^{\infty}\varphi_o(k_x,z-z')p(k_x,z')dz' \qquad (4a)$$

where

$$\varphi_o(k_x,z) = \int_{-\infty}^{\infty}\phi_o(x,z)\exp(2\pi ik_x x)dx$$

etc.

and the solution is given by

$$\rho(x,z) = \int_{-\infty}^{\infty} p(k_x,z)\exp(-2\pi ik_x x)dk_x \qquad (4b)$$

Equations (3) and (4) represent two methods of solving for $\rho(\underline{r})$. The former solves for the unknown $R(k_x,k_z)$ in frequency space and then inverse transforms in the k_x and k_z dimensions back to configuration space, whereas the latter tackles the problem in the k_x and z space followed by inverse transformation in the k_x dimension. Thereafter in the paper we shall refer to these methods as the deconvolution method [6,7], and the matrix method [9], respectively.

III. The Optical Transfer Function and the Undetermined Frequency Components

In order to reconstruct the object uniquely using the deconvolution method from Equation (3c), all the frequency components of the optical transfer function $\Phi_o(\underline{k})$ must be non-zero. For the matrix method, the corresponding requirement is that the integral operator in (4a) does not have zero as eigenvalues [10]. Neither of these two conditions holds when the ranges of integration involved cover all space and there is some plane passing through the origin of the point response function and that plane contains only one non-zero point. To show this, we first calculate the optical transfer function $\Phi_o(\underline{k})$. Due to the property of the positron camera event to be shown later (Equation (5)), we make the following coordinate transformation

$$r(x,z) \rightarrow r(\theta,z)$$

where $\theta = \tan^{-1}(\frac{x}{z})$

$$z = z$$

As mentioned in [6,7], the general point response function at (x,z) is defined as the number of straight lines, emitted from the point source, passing through a line segment of unit length at (x,z) oriented perpendicular to the z-axis weighted by a factor $F(\theta)$ depending on the angle the lines make with the z-axis. $F(\theta)$ is positive inside the cone and zero outside; the case of $F(\theta) = 1$ inside the cone corresponds to the conventional tomograms obtained from back-projecting the events. For $z \neq 0$, consider a line segment dx pointing along the x-axis centered at (θ,z) relative to the point source (Fig. 3a)

$$\phi_o(\theta,z) = F(\theta)\,\frac{\text{angle subtended by dx at origin}}{\pi}\,\frac{1}{dx}$$

$$= \frac{F(\theta)}{\pi}\,\frac{\cos^2\theta}{|z|}$$

Thus $\phi_o(\theta,z)|z| = \dfrac{F(\theta)\cos^2\theta}{\pi}$ ——————————— (5)

Equation (5) shows that $\phi_o(\theta,z)|z|$ is a function of θ only. This expression is valid also at $z = 0$. The optical transfer function is

$$\Phi_o(k_x,k_z) = \int_{-\infty}^{\infty} dz \int_{-\infty}^{\infty} dx \phi_o(x,z) \exp(2\pi i(k_x x + k_z z)) \qquad (6)$$

Performing this integral (Appendix A) we get

$$\Phi_o(k_x,k_z) = \begin{cases} \dfrac{\delta(z)}{\pi} \displaystyle\int_{-\theta_o}^{\theta_o} F(\theta)d\theta & \text{if } k_x = 0 \\[2ex] \dfrac{1}{\pi|k_x|} F(\theta_i)\cos^2\theta_i \quad \text{where } \tan\theta_i = \dfrac{-k_z}{k_x} & \text{if } k_x \neq 0 \end{cases}$$

Figure 3b shows schematically the shape of the two-dimensional optical transfer function. Three-dimensional point response functions and optical transfer functions are treated in Appendix B, and the result (B.3) for the pyramidal $\phi_o(\underline{r})$ is illustrated in Figure 4. Figures 3b and 4b show that there are regions in frequency space where $\Phi_o(\underline{k})$ is zero, and thus $R(\underline{k})$ cannot be recovered by the deconvolution method from Equation (3). Also note that Equations (A.2) and (B.2) show that the Φ_o of those point response functions satisfying Equations (5) and (B.1), respectively, are non-negative.

However, if the point response function in Figure 4a is rotated around the x-axis, a cylindrically-shaped point response function will be generated. Making use of the linearity of the Fourier transformation and the non-negativity of Φ_o, the corresponding optical transfer function can be obtained by rotating the function in Figure 4b around the k_x-axis. The resulting function in non-zero everywhere in the frequency space.

This example illustrates the following general principle:

"the necessary and sufficient condition for the optical transfer function in a positron camera to be non-zero everywhere is that every plane passing through the origin (the location of the point emitter) of the point response function contains at least a line of non-zero values." (7)

The proof is given in Appendix C.

In the case of the matrix method, we claim that the integral operator (4a) does have zero as its eignevalue for every value of k_x if condition (7) is not satisfied. First we show that $\{\exp(-2\pi i k_z z)\}$ is the set of eigenfunctions of the integral operator. Setting $p(k_x,z) = \exp(-2\pi i k_z z)$, the integral becomes

$$\int_{-\infty}^{\infty} \varphi_o(k_x, z-z')\exp(-2\pi i k_z z')dz'$$

$$= \exp(-2\pi i k_z z)\, \Phi_o(k_x,k_z)$$

Thus $\{\exp(-2\pi i k_z z)\}$ is the set of eigenfunctions for the integral operator with eigenvalues $\Phi_o(k_x,k_z)$. However, we have already shown that Φ_o has zero components if some cross-section of ϕ_o through the origin contains one non-zero point only. Since the eigenfunctions form a complete set, the general solution of the integral equation (4a) is

$$p(k_x,z) = \int_{-\infty}^{\infty} C(k_x,k_z)\exp(-2\pi i k_z z)dk_z$$

where the coefficients $C(k_x,k_z)$ are given by

$$C(k_x,k_z) = \begin{cases} \dfrac{\int_{-\infty}^{\infty} \varphi(k_x,z)\exp(2\pi i k_z z)dz}{\Phi_o(k_x,k_z)} = \dfrac{\Phi(k_x,k_z)}{\Phi_o(k_x,k_z)}, & \text{if } \Phi_o(k_x,k_z) \neq 0 \\ \text{undetermined, if } \Phi_o(k_x,k_z) = 0 \end{cases}$$

The solution $\rho(x,z)$ in configuration space is obtained by inverse transforming $p(k_x,z)$ in the k_x dimension, and it can be seen that the result is identical to that obtained by the deconvolution method, as expected.

It follows that $\rho(x,z)$ cannot be determined uniquely using either the deconvolution method or matrix method represented by Equations (3) and (4), respectively, when the point response function does not satisfy (7) and no further information is available.

IV. Use of A Priori Information

In this section we discuss the effect of some of the a priori constraints on the undetermined components of $R(\underline{k})$.

In all physically interesting situations we will be dealing with a bounded, finite object in which the appropriate density $\rho(\underline{r})$ is to be determined. Furthermore, due to the limitation in resolution of the measuring device and the fact that computation is usually done in a digital computer, this object distribution will be analyzed on a grid of points with finite spacings Δx, Δz. In order to understand the effect of each constraint separately, we will consider the following cases:

Finite Spacing

The vanishing of $\Phi_o(k_x,k_z)$ outside the cone in Figure 3b is due to the delta function property of the integral in (A.1), which in turn arises from the infinitesimal resolution in the z dimension of the point response function. If the assumption is made that the distribution of $\rho(x,z)$ in the z dimension is discrete, most of the zero components of $\Phi_o(\underline{k})$ will become non-zero through sampling, and hence the corresponding components of $R(\underline{k})$ will be recovered. The detailed analysis is done in Appendix D. The results show that the number of undetermined frequency components of $R(\underline{k})$ is greatly reduced if $\Delta z \neq 0$. Accordingly, the number of eignefunctions with zero as eigenvalue in the matrix method is also reduced.

Finite Extent of Object

By making use of the fact that the extent of the object is finite, all of the undetermined coefficients in the solution can be removed. This is a consequence of two theorems: (1) the Fourier transform of a finite object is an entire function, and (2) an entire function can be continued throughout the whole complex plane from a knowledge of the function on any finite continuous line segment [11]. We consider the effects of the finiteness of the object in two steps.

(a) Finiteness in z dimension ($z_1 < z < z_2$)

The Fourier transform $R(k_x,k_z)$ of $\rho(\underline{r})$ is entire in k_z. So, for any $k_{x_1} \neq 0$, the function $R(k_{x_1},k_z)$ can be calculated for all values of k_z from a knowledge of the function on the line segment $k_z \in (-k_{x_1}\tan\theta_o, k_{x_1}\tan\theta_o)$ (Figure 5). This cannot be done at $k_{x_1} = 0$, where the line segment degenerates into a point.

This process of analytic continuation in k_z can be carried out for any non-zero angle θ_o. The limiting case is when $\theta_o = 0$, where for every k_{x_1} the line segment $k_z \in (-k_{x_1}\tan\theta_o, k_{x_1}\tan\theta_o)$ degenerates into a point. For the general case $\theta_o \neq 0$, the only information that cannot be recovered is $R(0,k_z)$ with $k_z \neq 0$. Since $p(0,z)$ and $R(0,k_z)$ are a Fourier transform pair, and

$$p(0,z) = \int_{-\infty}^{\infty} \rho(x,z)dx$$

represent the total slice density on the z-plane, the undeterminacy of $R(0,k_z)$ where $k_z \neq 0$ means that the total slice density on each z-plane cannot be determined uniquely. However, the total object density is known, since

$$R(0,0) = \iint \rho(x,z)dxdz$$

is known.

As for the matrix method, the integral operator (4a) in this case becomes positive definite when the range of integration in z is finite. This can be seen as follows.

$$\varphi_o(k_x,z-z') = \int_{-\theta_o}^{\theta_o} \frac{F(\theta)}{\pi} \exp(2\pi i k_x \tan\theta(z-z'))d\theta$$

For any function f(z) piece-wise continuous and spatially bounded in $z_1 \leq z \leq z_2$,

$$\int_{z_1}^{z_2} dz' \int_{z_1}^{z_2} dz \varphi_o(k_x, z-z') f(z) \overline{f(z')}$$

$$= \int_{z_1}^{z_2} dz' \int_{z_1}^{z_2} dz \int_{-\theta_o}^{\theta_o} d\theta \frac{F(\theta)}{\pi} \exp(2\pi i k_x \tan\theta (z-z')) f(z) \overline{f(z')}$$

$$= \frac{1}{\pi} \int_{-\theta_o}^{\theta_o} F(\theta) \left| \int_{z_1}^{z_2} \exp(2\pi i k_x \tan\theta z) f(z) dz \right|^2 d\theta \qquad (8)$$

Since $F(\theta) > 0$ for all $-\theta_o \leq \theta \leq \theta_o$, the vanishing of expression (8) would require that

$$I(k_x \tan\theta) = \int_{z_2}^{z_1} \exp(2\pi i k_x \tan\theta z) f(z) dz = 0$$

$$\text{for all } -|k_x \tan\theta_o| \leq k_x \tan\theta \leq |k_x \tan\theta_o|$$

Now the integral $I(k_x \tan\theta)$ is an entire function [12]. If it is zero within the interval $[-k_x \tan\theta_o, k_x \tan\theta_o]$, it must be zero everywhere. Thus $f(z)$ must be zero everywhere. This argument proves that the integral operator

$$g(z) = \int_{z_1}^{z_2} \varphi_o(k_x, z-z') f(z') dz'$$

is positive definite, and by [10], the eigenfunctions associated with it form a complete set in the class of functions square integrable in (z_1, z_2), and thus unique solutions exist for the integral operator.

This argument breaks down if $k_x \tan\theta_o = 0$. Therefore, there is no unique solution for $p(k_x, z)$ if $k_x = 0$ or $\theta_o = 0$. For the general case $\theta_o > 0$, the only missing information is $p(0,z)$. As in the case of the deconvolution method, this implies that the total slice density on each z-plane cannot be determined. The total object density, however, can still be determined. This can be seen as follows:

$$\varphi_o(0,z) = \int_{-\infty}^{\infty} \phi_o(x,z) dx$$

$$= \int_{-\theta}^{\theta} \phi_o(\theta, z) |z| \sec^2\theta d\theta$$

$$= \int_{-\theta}^{\theta} \frac{F(\theta)}{\pi} d\theta \qquad \text{(from Equation (5))}$$

$= A(\theta_o)$ (say)

Substituting into (4a) with $k_x = 0$ we get

$$\varphi(0,z) = \int_{z_1}^{z_2} A(\theta_o)p(0,z')dz'$$

$$= A(\theta_o)\int_{-\infty}^{\infty}dx'\int_{z_1}^{z_2}dz'\rho(x',z')$$

Hence, total object density $= \int_{-\infty}^{\infty}dx'\int_{z_1}^{z_2}dz'\rho(x',z')$

$$= \frac{\varphi(0,z)}{A(\theta_o)}$$

<u>(b) Finiteness in both x and z dimensions</u>: $(x_1 \leq x \leq x_2,\ z_1 \leq z \leq z_2)$

In this case, $R(k_x,k_z)$ is entire in both k_x and k_z, so for the deconvolution method, $R(k_x,k_z)$ can be continued throughout the k-space from a knowledge of the function within the cone defined by any two intersecting line segments.

Again, the procedure cannot be used when $\theta_o = 0$, since then the only region in which $R(\underline{k})$ is known is the $k_z = 0$ line.

The above analysis shows that all the information of any density distribution of finite extent is contained in its Fourier components within any open cone in frequency space with its apex at the origin. This result is in agreement with the fact that such a distribution is uniquely determined by any infinite set of projections [13,14].

For the matrix method, the fact that $p(k_x,z)$ is entire in k_x for all $z_1 \leq z \leq z_2$ can be employed to fill up the undetermined components at $k_x = 0$ on each z-plane from values at $k_x \neq 0$ on the same z-plane.

If $\theta_o = 0$, the components at $k_x \neq 0$ ($k_z \neq 0$) are not known themselves, not to mention the continuation to $k_x = 0$.

In transmission imaging using parallel beams of x-rays and some other applications mentioned in Section I, the measured data are in the form of projections $P(r,\theta)$ of the object at certain angles θ. By the projection theorem [15], the one-dimensional Fourier transform of $P(r,\theta)$ in r gives the components of the two-dimensional Fourier transform of $\rho(x,z)$ on a line at angle $(\theta + \pi/2)$. If the projections are taken in a limited range of angle, we will get the Fourier components of $\rho(x,z)$ within a cone, giving rise to the situation shown in Figure 5. The process of analytic continuation given above can therefore be applied to obtain the rest of the Fourier components of $\rho(x,z)$.

V. Results

We have tested the results developed in the previous sections by performing studies on a computer-generated phantom. As the computations had to be done on digital computers, all the mathematical quantities were digitized on a lattice with cell size Δx, Δy, Δz, the choice of which is governed by the spatial resolution of the imaging device and the available core memory capacity of the computer. In digitizing we have restricted ourselves to frequency components below the maximum frequencies given by

$$k_x(\max) = \frac{1}{2\Delta x}, \text{ etc.}$$

The components at frequencies above this value are very small in magnitude as a consequence of the finite resolution, and will be placed equal to zero for computational purposes. The constraint that the density distribution is non-negative was also utilized in the reconstruction.

We first tested the effect of the size of the camera angle on the computer-generated phantom shown in Fig. 6, which is a spherical skull with a tumor located off-center inside. The skull is of inner radius 9 cm and thickness 2 cm, while the tumor has radius 1.5 cm. The concentration ratio is

tumor : skull : background = 10 : 5 : 1

We performed the reconstruction using the deconvolution method in three positron camera configurations with three different point response functions. The first point response function subtends a viewing angle (the solid angle of the detection cone in Fig. 4a) of one-third of 4π along the z-axis; the second one subtends two-thirds of 4π, one-third along the z-axis and the other third along the y-axis; and the last one has complete 4π viewing angle. They correspond to camera configurations having one, two, and three pairs of detectors, respectively, with the axes joining each pair perpendicular to each other. The last configuration, though not very realistic practically, was included for making comparisons, because its point response function obviously contains no zero Fourier components. According to condition (7) in Section III, the first point response function contains zero Fourier components, whereas the second one does not. The phantom generated a total number of 1.2 million events in each case. Reconstructions were done on a 48 x 48 x 48 lattice, with cell size equal to 1 cm x 1 cm x 1 cm. Each event was weighed by $F(\theta) = \cos^{-3}\theta$ in constructing $\phi(\underline{r})$.

In the presence of noise, Equation (3c) is modified to

$$R(\underline{k}) = \frac{\Phi_o(\underline{k})}{\Phi_o(\underline{k}) + \frac{\gamma(2\pi)^4 k^4}{\Phi_o(\underline{k})}} \qquad (9)$$

by the smoothing algorithm developed in [6].

Besides suppressing the noise in the high frequency range, Equation (9) also has the effect of setting the values of $R(\underline{k})$ to zero in the region of frequency space where $\Phi_o(\underline{k}) = 0$. This property can be expected from the smoothness constraint imposed upon the solution, since in the absence of any

information on the amplitude vector $R(\underline{k})$ of the sinusoidal wave at frequency $\underline{k}$, setting $R(\underline{k})$ to zero gives a solution $\rho(\underline{r})$ with minimum fluctuation. This $R(\underline{k})$, however, is clearly not the correct solution, since it is not an analytic function as it is discontinuous at the edge of the allowed cone (see Fig. 4b).

Figs. 7, 8 and 9 show the reconstructions obtained, and Table I shows the optimum value of σ in each of the configurations, where σ is a measure of the deviation of the reconstruction from the object, given by

$$\sigma = \sqrt{\sum_{i,j,k} (\text{reconstruction}(i,j,k) - \text{phantom}(i,j,k))^2}$$

It can be seen that the reconstruction from deconvolution using the four-sided camera point response function is essentially identical to that using the point response function with 4π viewing angle, showing clearly that the Fourier components of the four-sided camera point response function are also non-zero everywhere. On the other hand, the two-sided camera point response function gives a reconstruction considerably worse than that of the other two, as can be expected from the presence of zero components in its Fourier transform.

Next we investigated the effect of the finite extent of the object in extending the spectrum $R(\underline{k})$ beyond the allowed cone for the first camera configuration (two detectors: 1/3 x 4π viewing angle). The iterative scheme shown in Fig. 10 was employed to this end. The spectrum $R^{(0)}(\underline{k})$ obtained from deconvolution was Fourier-transformed to the object space. There the values outside the known extent of the object were set to zero, and then inverse-transformed to the frequency space, giving $R^{(1)}(\underline{k})$. The components of $R^{(1)}(\underline{k})$ inside the allowed cone were reset to the original values given by $R^{(0)}(\underline{k})$, and the cycle repeated, yielding $R^{(n)}(\underline{k})$ after n iterations.

We note that this iterative scheme has been used by Gerchberg [16] and Papoulis [17] to improve the resolution of one-dimensional signals in band-limited systems. The convergence of the scheme in one dimension has been proved by both of these authors. The proof given in Gerchberg's paper made use of the property that a real analytic function in one-dimensional space either vanishes everywhere or only has isolated zeros. This proof can be generalized to higher dimensions by using the more general property that real analytic functions on n-dimensional space cannot vanish on an infinite set of n-1 dimensional planes through the origin without vanishing identically.

Fig. 11 shows the reconstruction in the first camera configuration after 15 iterations, and Fig. 12 shows the values of σ as a function of the number of iterations. It can be seen that the scheme converges at about 15 iterations, and the value of σ is reduced to a level much closer to, though still higher than, that obtained using the point response function with 4π viewing angle, there being a factor of three in the reduction of the difference in σ. The residual difference is attributed to the propagation of errors in iterating, from such sources as statistical fluctuation, and aliasing and leakage in performing digital Fourier transform [18].

VI. Conclusion

We have shown that, in principle, one can reconstruct the object completely no matter how small the solid angle the imaging device subtends, provided one makes use of a priori information. However, the noise in the data poses a practical limit to the quality of the reconstruction. The errors in the reconstruction due to noise propagation become serious in the case when the solid angle of the imaging device becomes too small. Our computer simulations have shown that imaging with solid angle 4 steradian provides adequate reconstructions. Imaging with solid angles of this size occurs in applications in other fields such as electron microscopy.

A detailed comparison of the relative costs and tradeoffs between the imaging solid angle and the computational and statistical errors will be covered in a forthcoming paper.

Acknowledgments

This work was supported by the Physics Division of the Department of Energy under contract No. W-7405-ENG-48 and by the National Institute of Health.

Table I

Reconstructions Using the Deconvolution Method

Number of detectors in the positron camera	2	4	6
Optimum σ	1.000	0.712	0.704

Appendix A

$$\Phi_o(k_x,k_z) = \int_{-\infty}^{\infty} dz \int_{-\infty}^{\infty} dx\ \phi_o(x,z)\ \exp(2\pi i(k_x x + k_z z))$$

$$= \int_{-\infty}^{\infty} dz \int_{-\pi}^{\pi} d\theta\ \phi_o(\theta,z)\ \exp(2\pi i z(k_x \tan\theta + k_z))|z|\sec^2\theta$$

$$= \int_{-\theta_o}^{\theta_o} d\theta\ \frac{F(\theta)}{\pi} \int_{-\infty}^{\infty} dz\ \exp(2\pi i z(k_x \tan\theta + k_z))$$

Now

$$\int_{-\infty}^{\infty} \exp(2\pi i z(k_x \tan\theta + k_z))dz = \delta(k_x \tan\theta + k_z) \qquad \text{(A.1)}$$

therefore

$$\Phi_o(k_x,k_z) = \int_{-\theta_o}^{\theta_o} \frac{F(\theta)}{\pi}\ \delta(k_x \tan\theta + k_z)d\theta$$

$$= \begin{cases} \dfrac{\delta(k_z)}{\pi}\displaystyle\int_{-\theta_o}^{\theta_o} F(\theta)d\theta & \text{if } k_x = 0 \\[2ex] \dfrac{F(\theta_i)\cos^2\theta_i}{\pi|k_x|} & \text{if } k_x \neq 0 \end{cases} \qquad \text{(A.2)}$$

where $\tan\theta_i = -\dfrac{k_z}{k_x}$

Appendix B

In three-dimension, equation (5) takes the form

$$\phi_o(\underline{s},z)|z|^2 = H(\underline{s}/z) \qquad \text{(B.1)}$$

where $\underline{s}=(x,y)$, and the angular function H is positive inside the data cone and zero outside. Defining $\underline{t} = \underline{s}/z$, $\underline{w} = (k_x,k_z)$, and performing the Fourier transformation, we get

$$\Phi_o(\underline{w},k_z) = \int dz \iint d^2s\ \phi_o(\underline{s},z)\ \exp(2\pi i(\underline{w}\cdot\underline{s}+k_z z))$$

$$= \iint H(\underline{t})\ \delta(\underline{w}\cdot\underline{t}+k_z)d^2t$$

The vector $\underline{t} = (t_1,t_2)$ can be chosen so t_1 lies along $\underline{w}$, giving $\underline{w}\cdot\underline{t}+k_z=|\underline{w}|t_1+k_z$. Then we get

$$\Phi_o(\underline{w},k_z) = \begin{cases} \delta(k_z) \iint H(\underline{t})d^2t & \text{if } \underline{w} = 0 \\ \int H(-k_z/|\underline{w}|,t_2)dt_2 & \text{if } \underline{w} \neq 0 \end{cases} \qquad \text{(B.2)}$$

In the particular case where ϕ_o is in the form of a square pyramid, ie.

$\phi_o(x,y,z) \neq 0$ whenever $0 \leq |x| \leq |z\tan\theta_o|$

and $0 \leq |y| \leq |z\tan\theta_o|$

application of (B.2) shows that

$$\Phi_o(k_x,k_y,k_z) > 0 \text{ if } |k_x| + |k_y| > |k_z|/\tan\theta_o \quad \text{when } |k_x|,\ |k_y| > 0$$

$$\text{or } |k_x| + |k_y| \geq |k_z|/\tan\theta_o \quad \text{when } |k_x|=0 \text{ or } |k_y|=0 \qquad \text{(B.3)}$$

$$= 0 \text{ otherwise}$$

Appendix C

In this appendix we prove the statement (7), namely, the necessary and sufficient condition for an optical transfer function to be non-zero everywhere is that every plane passing through the origin of the corresponding point response function contains at least a line of non-zero values.

Necessity

If there is a plane A through the origin of ϕ_o on which only the origin is non-zero, then we take the normal to A at the origin to be the z-axis. Equation (B.2) shows that Φ_o is zero on the k_z-axis except at the origin.

Sufficiency

Given a point response function satisfying condition (7), we want to show that the value of Φ_o at any arbitray point P in the frequency space is non-zero. First rotate the coordinate system in frequency space so that P lies on the k_x-axis. The plane x = 0 of ϕ_o contains at least one line with non-zero values. Take any such line to be the z-axis. Then decompose ϕ_o into two parts in the following manner:

$$\phi_o^{(1)}(x,y,z) = \begin{cases} 0 & \text{if } z = 0 \\ \phi_o(x,y,z) & \text{if } z \neq 0 \end{cases}$$

$$\phi_o^{(2)}(x,y,z) = \begin{cases} \phi_o(x,y,z) & \text{if } z = 0 \\ 0 & \text{if } z \neq 0 \end{cases}$$

Clearly $\phi_o = \phi_o^{(1)} + \phi_o^{(2)}$. Since $\phi_o^{(1)}$ satisfies (B.1), equation (B.2) shows that $\Phi_o^{(1)} > 0$, because $H(\underline{t}) > 0$ at $\underline{t} = 0$. Now it remains to show that $\Phi_o^{(2)}$ is non-negative at P. $\phi_o^{(2)}$ can be written as

$$\phi_o^{(2)}(s,\theta, z) = \frac{F(\theta)\ \delta(z)}{s}$$

where we have made the coordinate transformation $r(x,y) \rightarrow r(s,\theta)$. Transforming $k(k_x,k_y)$ to polar coordinate $k(w,\alpha)$, and taking the Fourier transform of $\phi_o^{(2)}$, we get

$$\Phi_o^{(2)}(w,\alpha,k_z) = \iiint \frac{F(\theta)\ \delta(z)}{s} \exp(2\pi i(sw\cos(\theta-\alpha)+k_z z))sdsd\theta dz$$

$$= \frac{F(\alpha+\pi/2)}{2\pi|w|}$$

which is clearly non-negative.

Appendix D

Let us represent the object $\rho(\underline{r})$ by

$$\Delta z \sum_{n=-\infty}^{\infty} \rho(x, n\Delta z)\ \delta(z - n\Delta z)$$

In this case the point response function $\phi_o(x,z)$ can be sampled in the z dimension in a corresponding manner

$$\phi_o(x,z) \rightarrow \Delta z \sum_{n=-\infty}^{\infty} \phi_o(x,z)\ \delta(z - n\Delta z)$$

Substituting the sampled $\phi_o(x,z)$ into Equation (6) yields

$$\Phi_o(k_x, k_z) = \int_{-\theta_o}^{\theta_o} \frac{F(\theta)}{\pi}\ \Delta z\ \left(\sum_{n=-\infty}^{\infty} \exp(2\pi i n \Delta z(k_x \tan\theta + k_z))\right) d\theta$$

From [19]

$$\sum_{n=-\infty}^{\infty} \exp(2\pi i n \Delta z(k_x \tan\theta + k_z)) = \frac{1}{\Delta z} \sum_{n=-\infty}^{\infty} \delta\left(k_x \tan\theta + k_z - \frac{n}{\Delta z}\right)$$

Thus

$$\Phi_o(k_x, k_z) = \sum_{n=-\infty}^{\infty} \int_{-\theta_o}^{\theta_o} \frac{F(\theta)}{\pi}\ \delta\left(k_x \tan\theta + k_z - \frac{n}{\Delta z}\right) d\theta$$

$$= \frac{1}{\pi |k_x|} \sum_{m \in M} F(\theta_m) \cos^2 \theta_m$$

where M is the set of integers m such that

$$k_x \tan\theta_m + k_z - \frac{m}{\Delta z} = 0 \quad \text{for some } -\theta_o \leq \theta_m \leq \theta_o$$

Since $F(\theta) \cos^2\theta > 0$ for all $0 \leq |\theta| \leq \theta_o$, it is enough to show

the set M non-empty for $\phi_o(k_x,k_z)$ to be non-zero. For frequency components inside the cone, ie., $|k_z| \leq |k_x|\tan\theta_o$, we have

$$k_x \tan\theta_m + k_z = 0 \quad \text{where } \tan\theta_m = \frac{-k_z}{k_x} \quad (\text{set } \theta_m = 0 \text{ if } k_x = 0)$$

thus $m = 0 \in M$, and therefore $\Phi_o(k_x,k_z)$ is non-zero.

For frequency components outside the cone,ie., $|k_z| > |k_x|\tan\theta_o$, it can be shown that

$$\Phi_o(k_x,k_z) \neq 0 \quad \text{if } |k_x| \geq 1/(2\tan\theta_o \Delta z)$$

otherwise $\Phi_o(k_x,k_z)$ is zero at a fraction of points on the line k_x =constant, and this fraction is given by

$$1 - 2\tan\theta_o \Delta z |k_x| \ .$$

References

[1] Robertson, J. S., Marr, R. B., Rosenblum, M., Radeka, V., and Yamamoto, Y. L., 1973, in: Tomographic Imaging in Nuclear Medicine, Ed. G. S. Freedman (New York: Society of Nuclear Medicine) pp.142-153.

[2] Hounsfield, G. N., Br. J. Radiol., 46 (1973) 1016-1022.

[3] McCullough, E. C., Payne,J. T., Baker, H. L., Hattery, R. R., Sheedy, R. F., Stephens, D. F., and Gedgaudus, E., Radiology, 120 (1976) 173-188.

[4] Lim,C. B., Chu, D., Kaufman, L., Perez-Mendez, V., Hattner, R., and Price, D. C., IEEE Trans. Nucl. Sci., NS-22 (1975) 388-394.

[5] Grant, D. G., IEEE Trans. Biomed. Eng., BME-19 (1972) 20-28.

[6] Chu, G., and Tam, K. C., Phys. Med. Biol., 22 (1977) 245-265.

[7] Tam, K. C., Chu, G., Perez-Mendez, V., and Lim, B. C., IEEE Trans.Nucl. Sci., NS-25 (1978) 152-159.

[8] Morse, P. M., and Feshbach, H., 1953, Methods of Theoretical Physics (New York: McGraw-Hill) Part I: chapter 8.

[9] Chang, L. T., Macdonald, B., and Perez-Mendez, V., IEEE Trans. Nucl. Sci., NS-23 (1976) 568.

[10] Riesz, F., and Sz.-Nagy, B., 1955, Functional Analysis (New York: Frederick Ungar) chapter 6.

[11] Harris, J. L., J. Opt. Soc. Am., 54 (1964) 931-936.

[12] Whittaker, E. T., and Watson, G. N., 1952, A Course of Modern Analysis (England: Cambridge University Press) p.67.

[13] Solmon, D. C., J. Math. Anal. Appl., 56 (1976) 61-83.

[14] Smith, K. T., Solmon, D. C., and Wagner, S. L., Bull. Amer. Math. Soc., 83 (1977) 1227-1270.

[15] Crowther, R. A., DeRosier, D. J., and Klug, A., Proc. Roy. Soc. Lond. A, 317 (1970) 319-340.

[16] Gerchberg, R. W., Optica Acta, 21 (1974) 709-720.

[17] Papoulis, A., IEEE.Trans. Circuits Syst., CAS-22 (1975) 735-742.

[18] Brigham, O., 1974, The Fast Fourier Transform (New York: Prentice Hall) chapter 6.

[19] Papoulis, A., 1962, The Fourier Integral and Its Applications (New York: McGraw-Hill) p.44.

Figure Captions

Figure 1. Two-dimensional imaging devices.

Figure 2. Three-dimensional imaging devices.

Figure 3. A two-dimensional point response function $\phi_o(\underline{r})$ and its optical transfer function $\Phi_o(\underline{k})$.

Figure 4. A pyramidal three-dimensional point response function $\phi_o(\underline{r})$ and its optical transfer function $\Phi_o(\underline{k})$.

Figure 5. Analytic continuation of $R(k_x,k_z)$ in k_z dimension.

Figure 6. A computer-generated phantom simulating a brain tumor. The skull is 2 cm thick and has an inner radius of 9 cm. The tumor has a radius of 1.5 cm. The concentration is 5 : 1 for the skull and 10 : 1 for the tumor. Each picture element is 1 x 1 cm^2. The planes are 1 cm apart in the z-direction.

Figure 7. Reconstructions from deconvolution using a point response function with viewing angle one-third of 4π along the z-axis. Each event is weighed by $\cos^{-3}\theta$ in constructing ϕ. The value of γ is 1.15×10^{-7}.

Figure 8. Reconstructions from deconvolution using a point response function with viewing angle one-third of 4π along the z-axis and one-third of 4π along the y-axis. Each event is weighed by $\cos^{-3}\theta$ in constructing ϕ. The value of γ is 1.54×10^{-7}.

Figure 9. Reconstructions from deconvolution using a point response function with complete 4π viewing angle. Each event is weighed by $\cos^{-3}\theta$ in constructing ϕ. The value of γ is 3.85×10^{-7}.

Figure 10. Iterative scheme to extend the spectrum $R(\underline{k})$ beyond the deconvolution region.

Figure 11. Reconstructions in Figure 7 after 15 iterations using the scheme shown in Figure 10.

Figure 12. The values of the mean square deviation of the reconstructions as a function of the number of iterations.

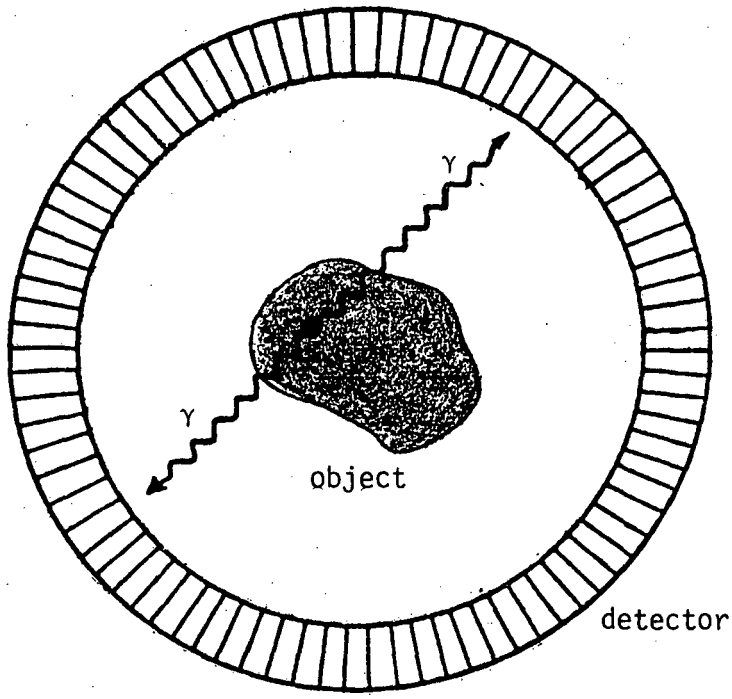

a. Ring positron camera

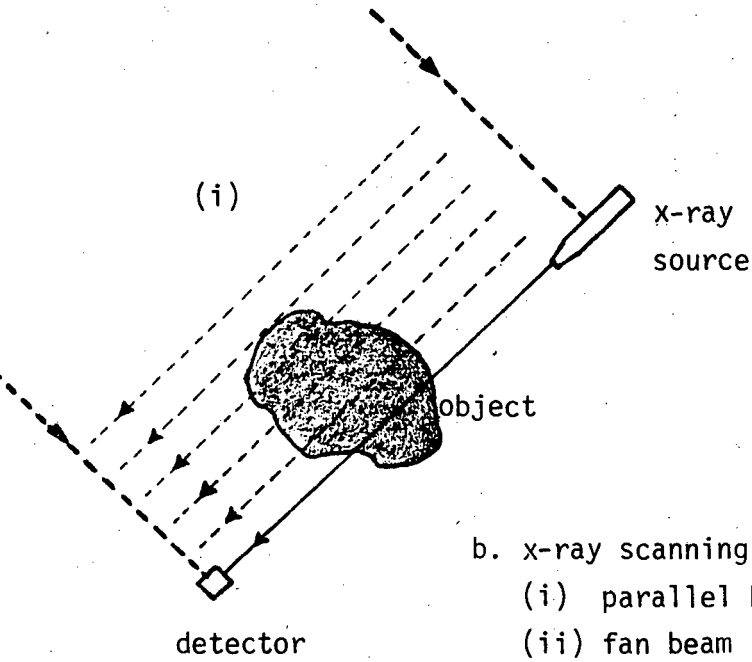

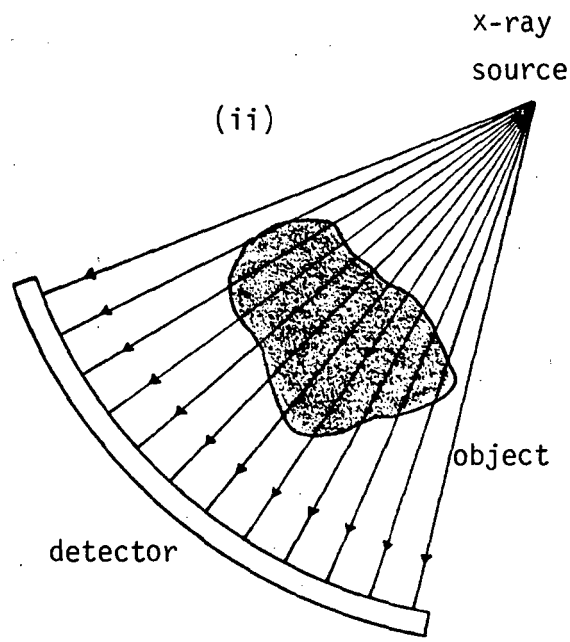

b. x-ray scanning
(i) parallel beam
(ii) fan beam

Figure 1

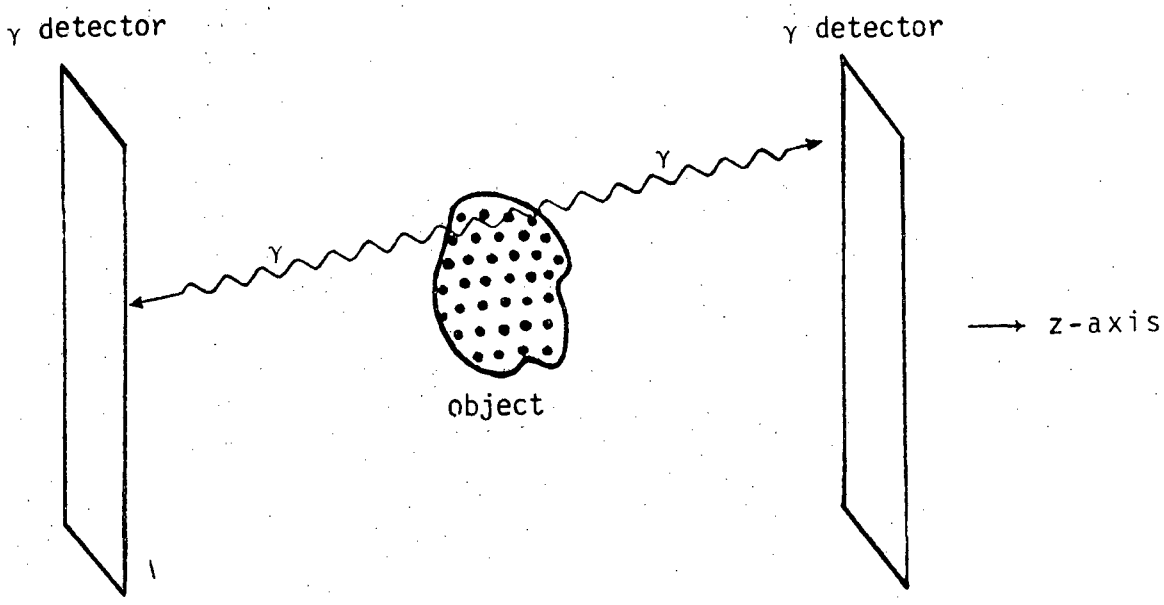

a. Planar positron camera

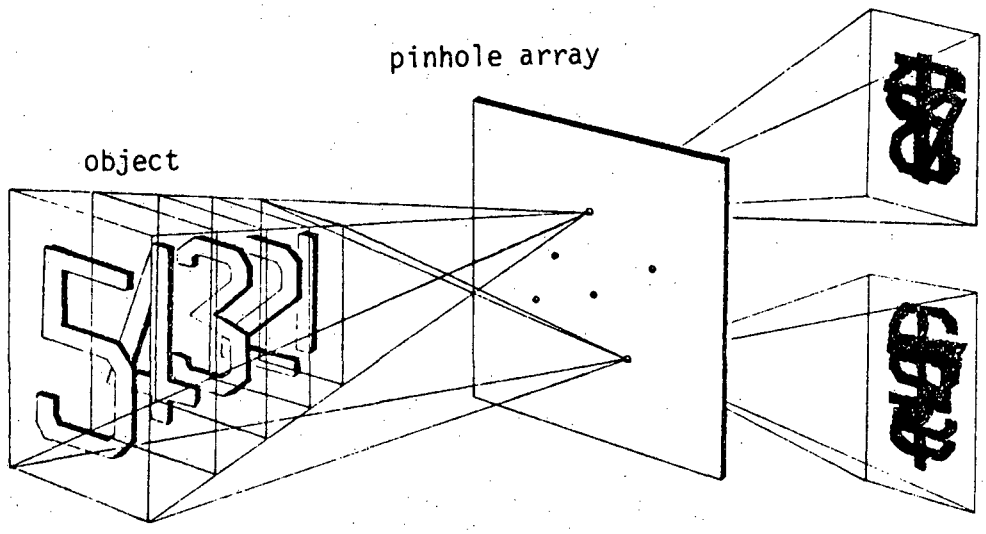

b. Pinhole imaging device

XBL 7812-13269

Figure 2

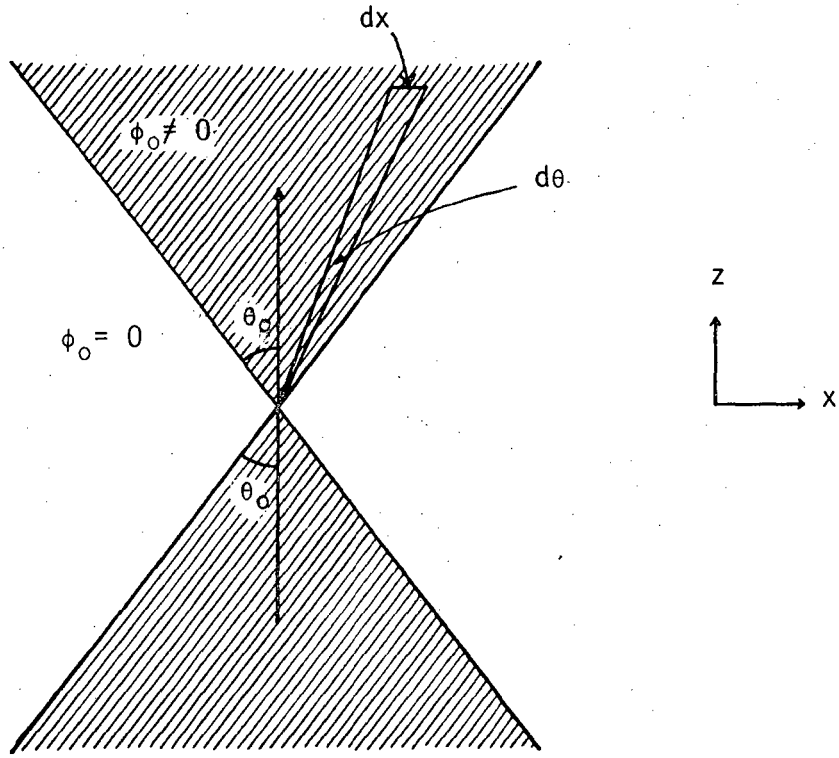

a. $\phi_o(\underline{r})$

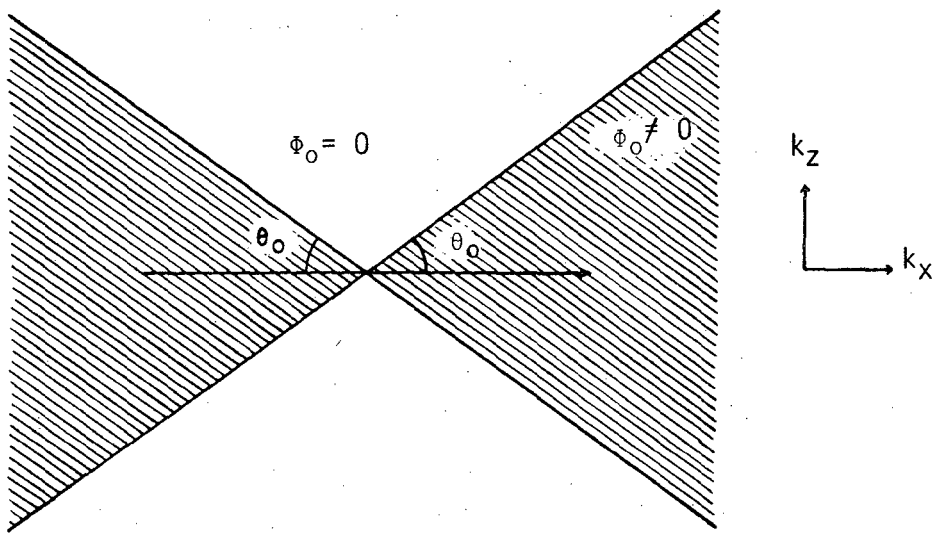

b. $\Phi_o(\underline{k})$

XBL 7812-13988

Figure 3

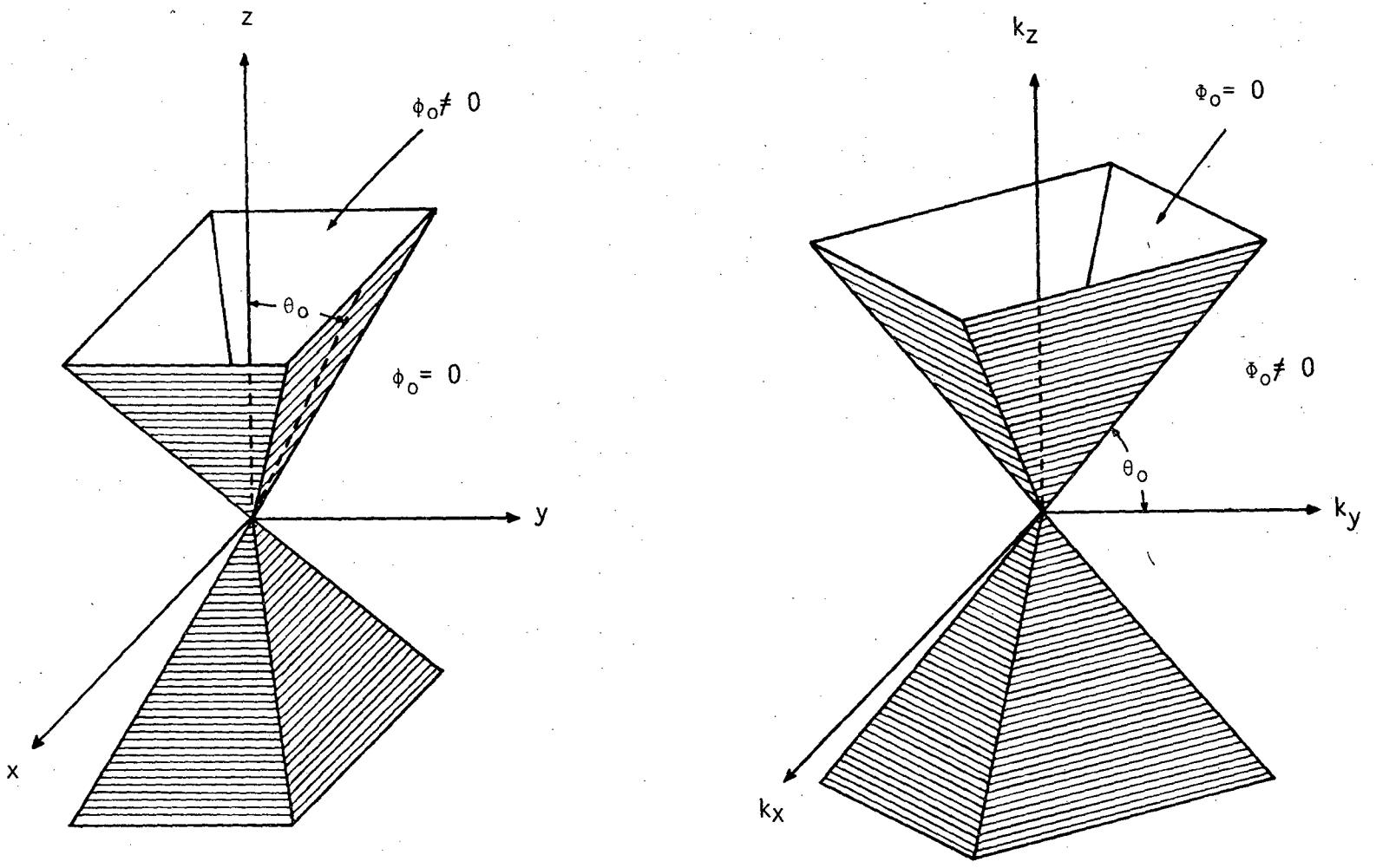

a. $\phi_o(\underline{r})$

b. $\Phi_o(\underline{k})$

XBL 7812-13270

Figure 4

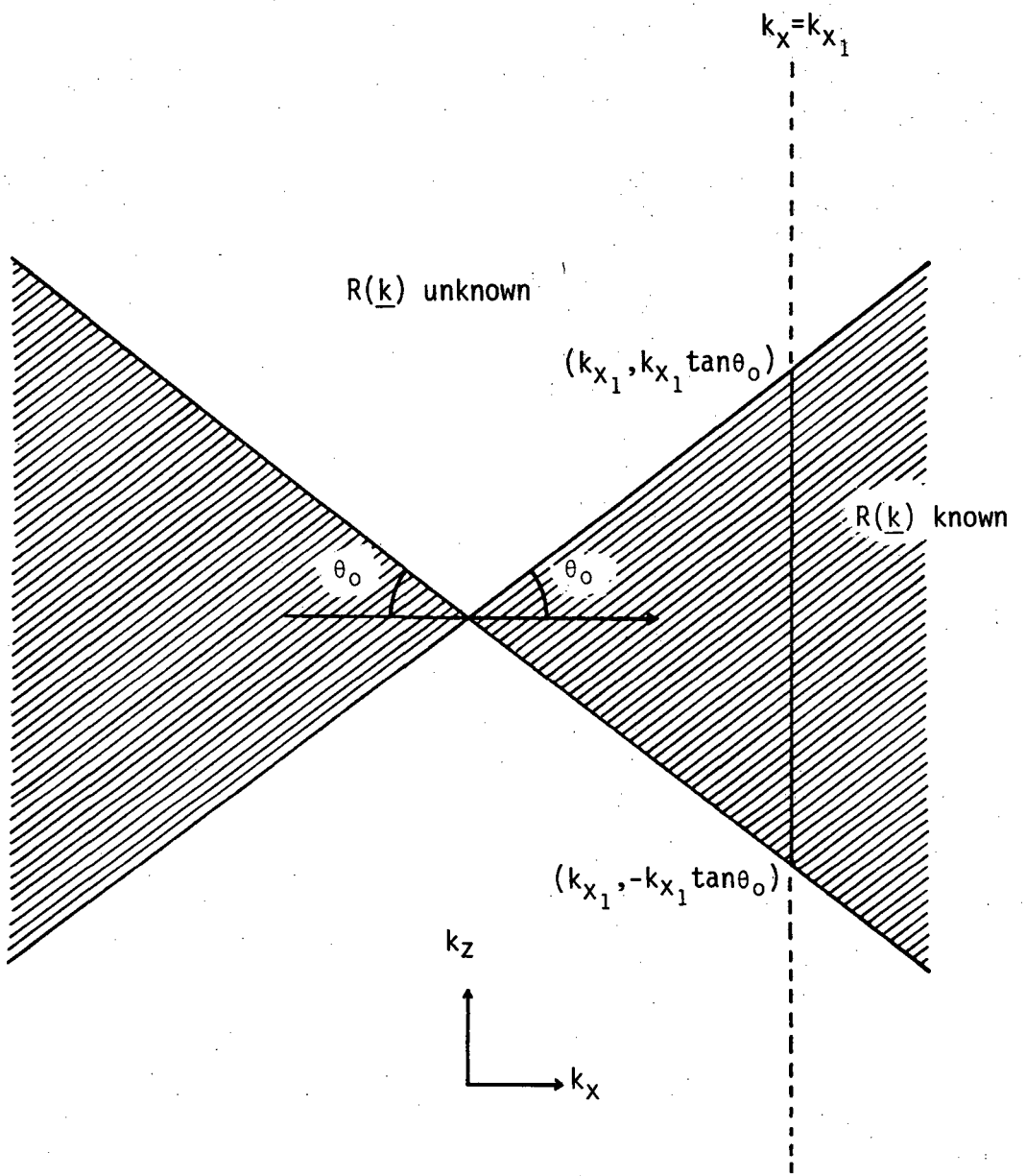

Figure 5

XBL 7812-13987

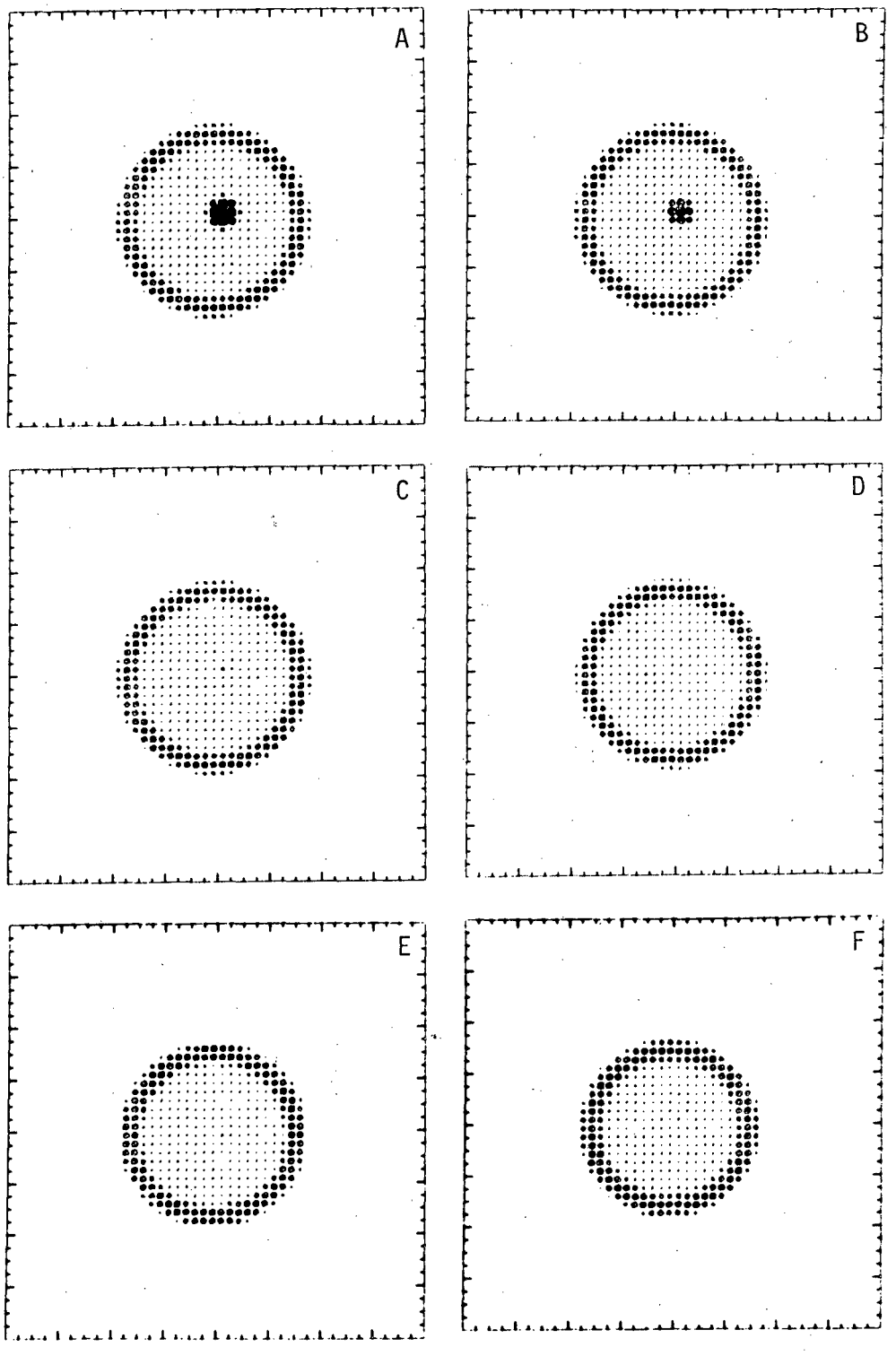

XBL 792-8263

Figure 6

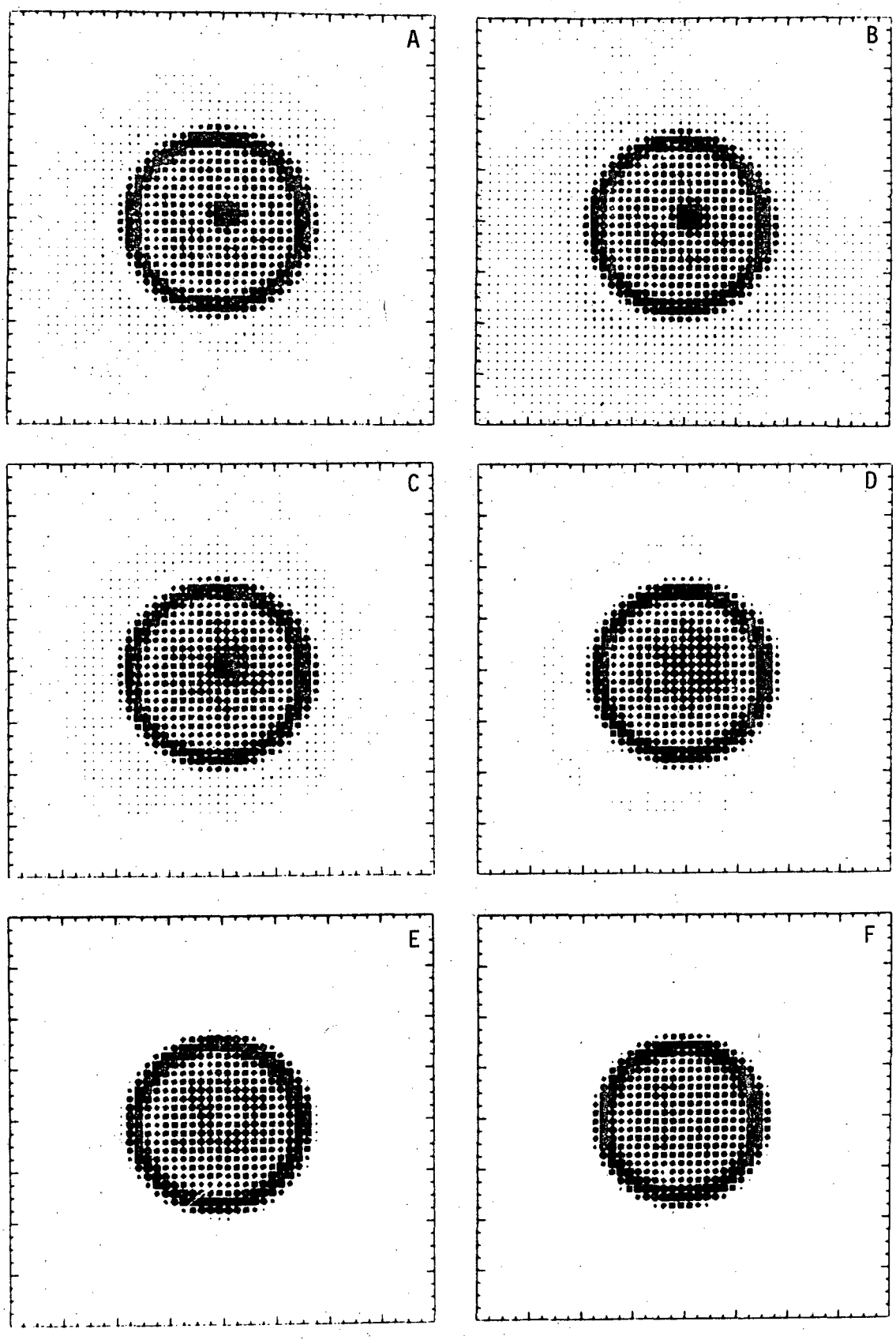

Figure 7

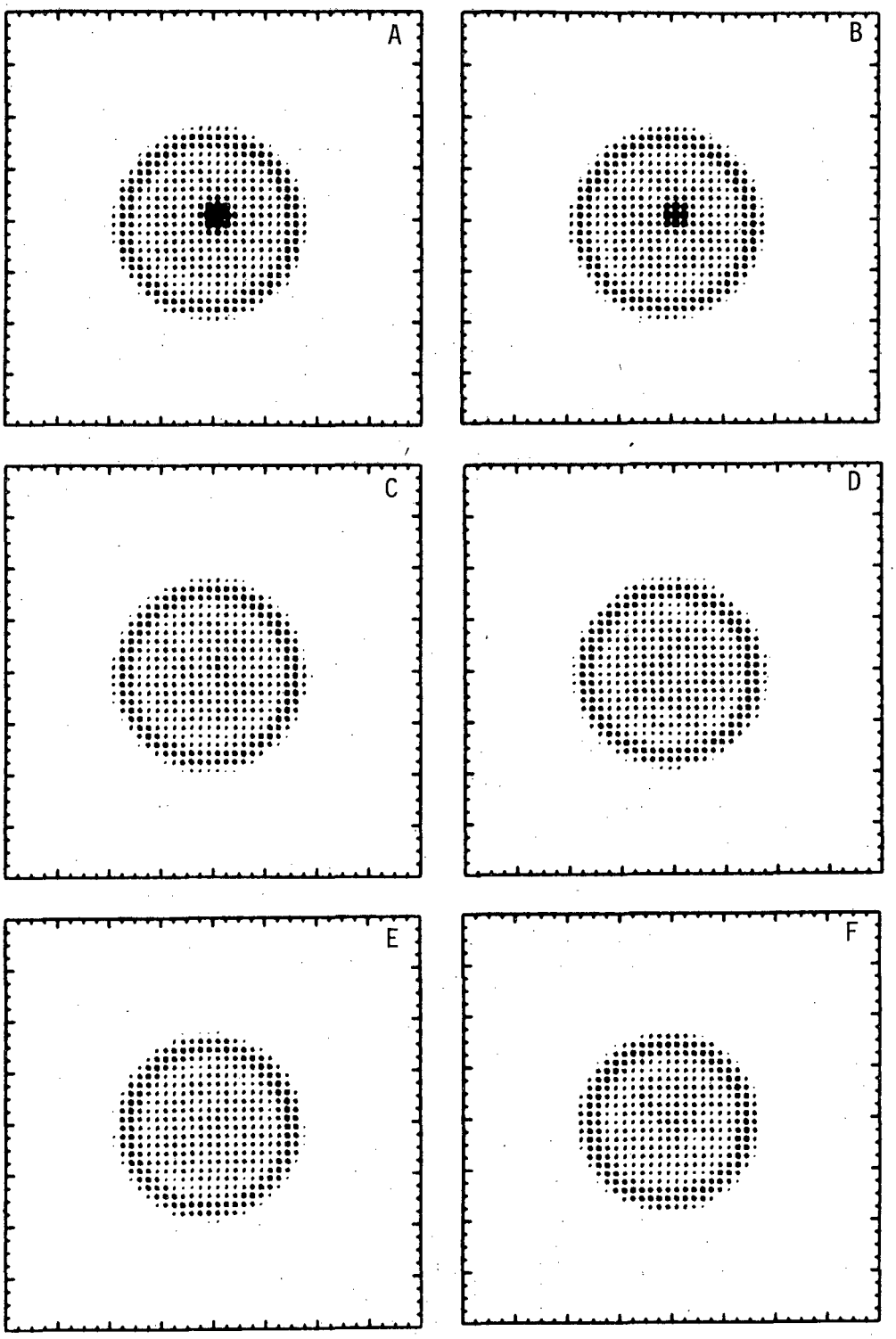

XBL 7812-14003

Figure 8

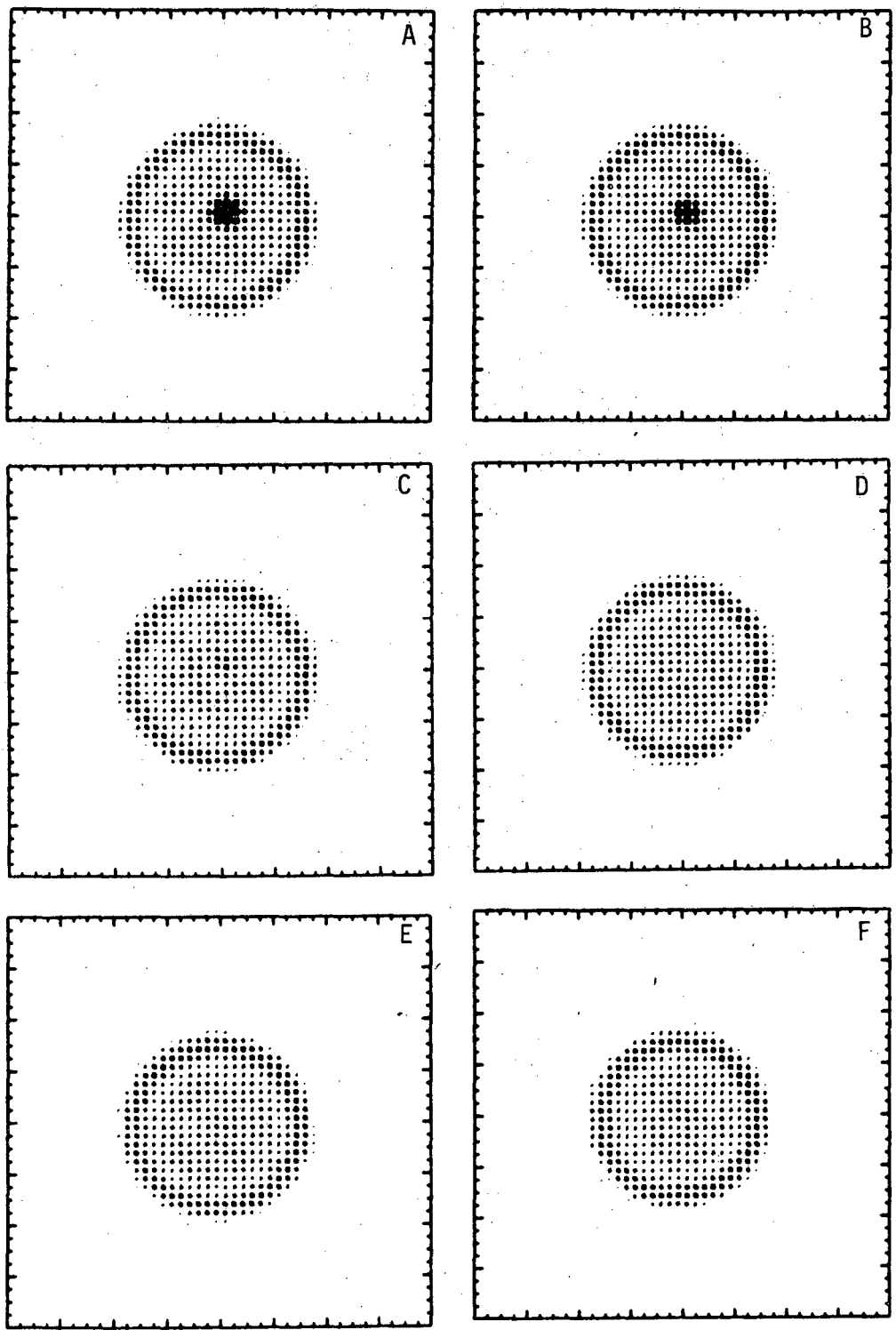

XBL 7812-14001

Figure 9

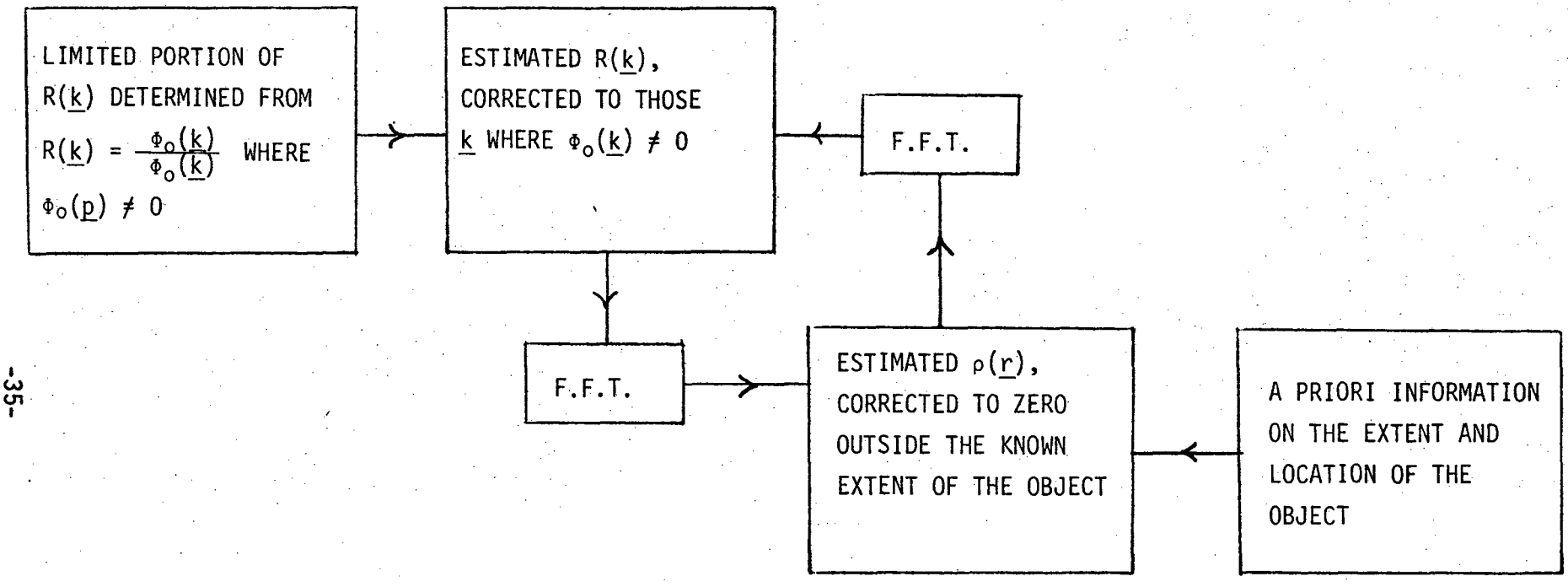
LIMITED PORTION OF
R(k) DETERMINED FROM
R(k) = Φo(k) / Φo(k) WHERE
Φo(p) ≠ 0
ESTIMATED R(k),
CORRECTED TO THOSE
k WHERE Φo(k) ≠ 0
F.F.T.
F.F.T.
ESTIMATED ρ(r),
CORRECTED TO ZERO
OUTSIDE THE KNOWN
EXTENT OF THE OBJECT
A PRIORI INFORMATION
ON THE EXTENT AND
LOCATION OF THE
OBJECT

Figure 10

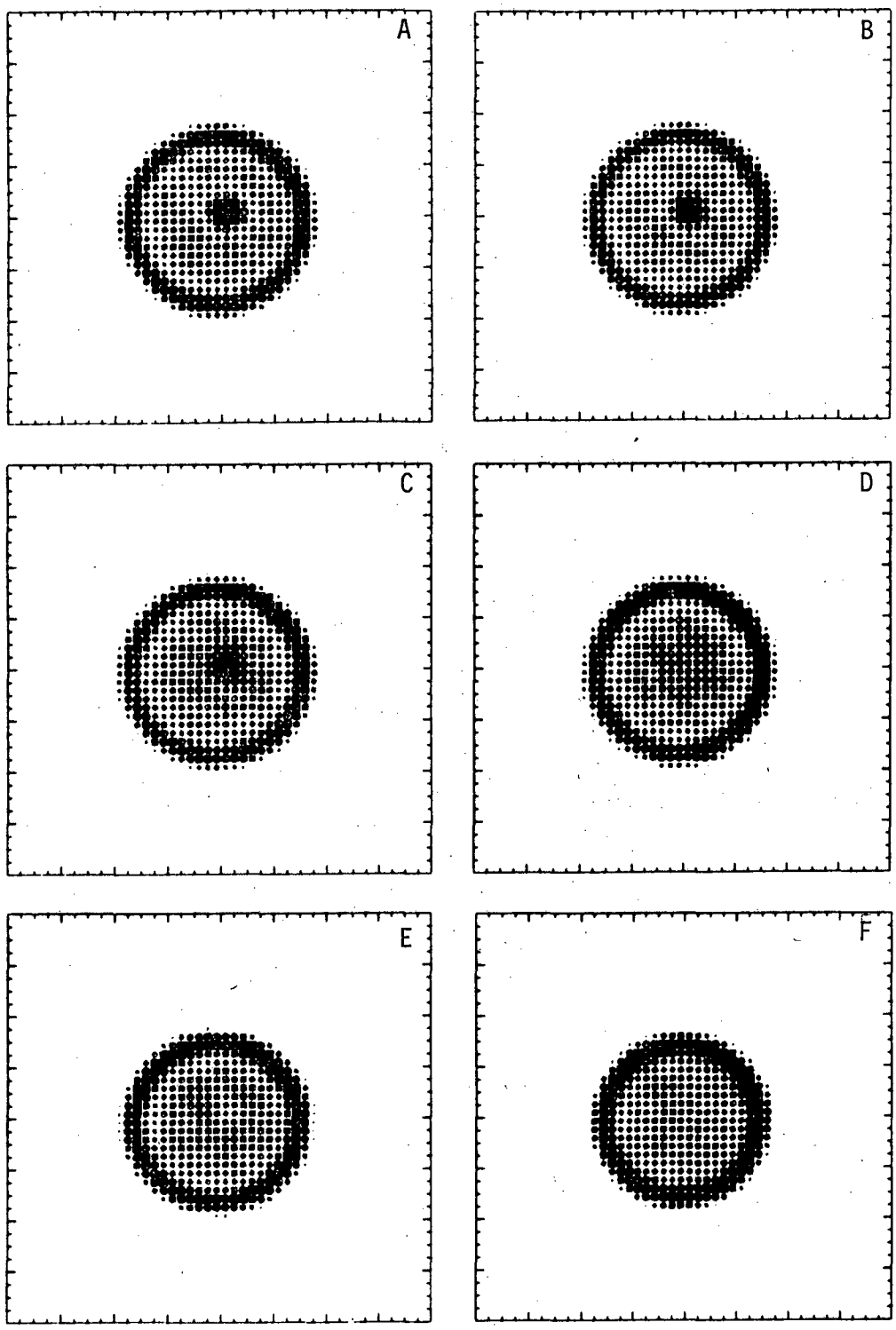

XBL 7812-13266

Figure 11

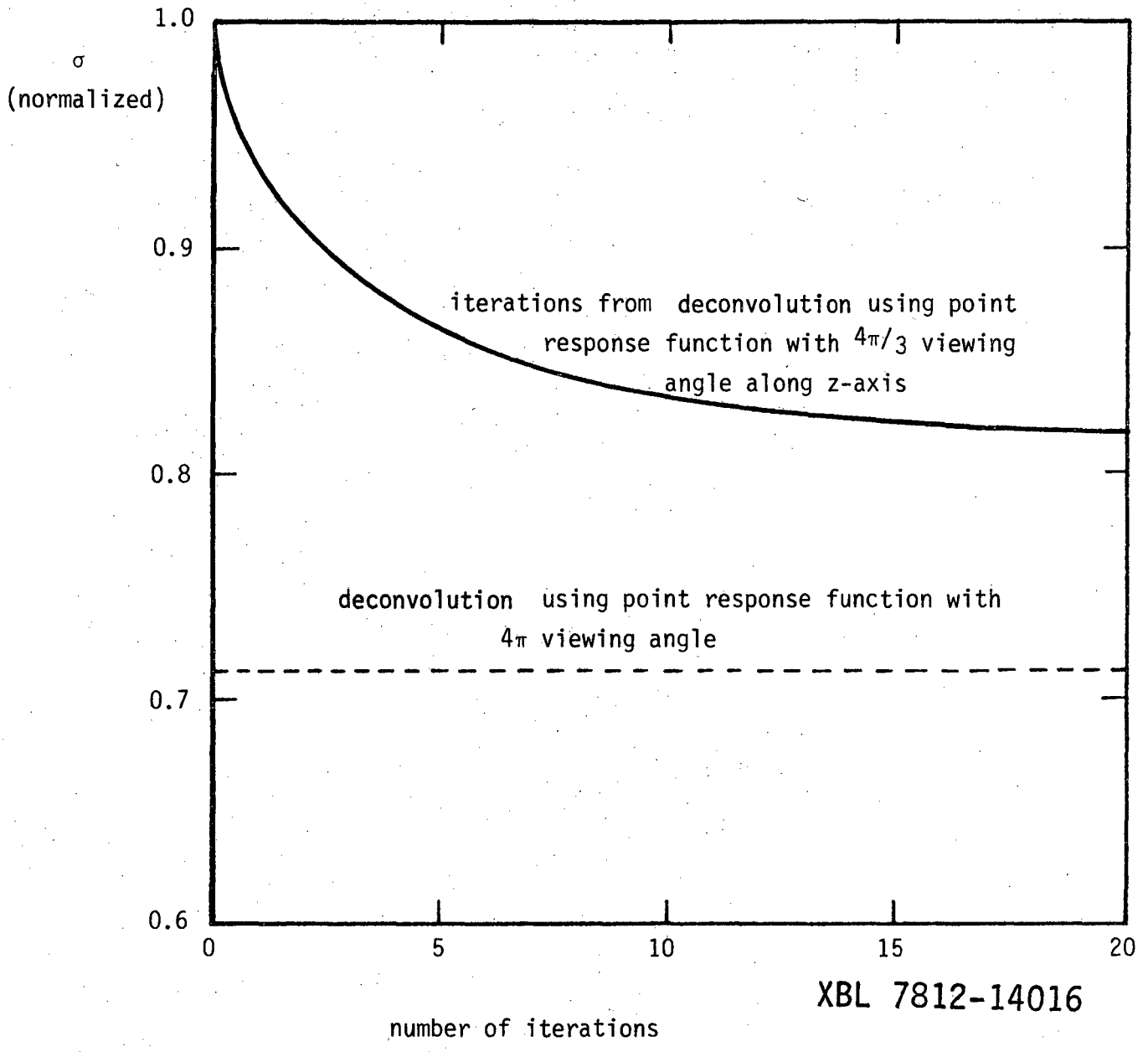
1.0
σ
(normalized)
0.9
0.8
0.7
0.6
iterations from deconvolution using point response function with 4π/3 viewing angle along z-axis
deconvolution using point response function with 4π viewing angle
0
5
10
15
20
XBL 7812-14016
number of iterations

Figure 12

This report was done with support from the Department of Energy. Any conclusions or opinions expressed in this report represent solely those of the author(s) and not necessarily those of The Regents of the University of California, the Lawrence Berkeley Laboratory or the Department of Energy.

TECHNICAL INFORMATION DIVISION
LAWRENCE BERKELEY LABORATORY
UNIVERSITY OF CALIFORNIA
BERKELEY, CALIFORNIA 94720